Geomechanics and Engineering, *Vol. 29, No. 6 (2022) 627-643*
https://doi.org/10.12989/gae.2022.29.6.627

Mechanical behavior of sandstones under water-rock interactions

Kunyou Zhou*[1,2], Linming Dou**[1,2], Siyuan Gong[2], Yanjiang Chai[2], Jiazhuo Li[2], Xiaotao Ma[2] and Shikang Song[3]

[1]*Key Laboratory of Deep Coal Resource Mining, Ministry of Education, China University of Mining and Technology, Xuzhou, Jiangsu, 221116, China*
[2]*School of Mines, China University of Mining and Technology, Xuzhou, Jiangsu, 221116, China*
[3]*Shaanxi Zhengtong Coal Industry Co., Ltd., Xianyang, Shaanxi, 713600, China*

(Received August 30, 2021, Revised April 15, 2022, Accepted May 3, 2022)

Abstract. Water-rock interactions have a significant influence on the mechanical behavior of rocks. In this study, uniaxial compression and tension tests on different water-treated sandstone samples were conducted. Acoustic emission (AE) monitoring and micro-pore structure detection were carried out. Water-rock interactions and their effects on rock mechanical behavior were discussed. The results indicate that water content significantly weakens rock mechanical strength. The sensitivity of the mechanical parameters to water treatment, from high to low, are Poisson ratio (μ), uniaxial tensile strength (UTS), uniaxial compressive strength (*UCS*), elastic modulus (E), and peak strain (ε). After water treatment, AE activities and the shear crack percentage are reduced, the angles between macro fractures and loading direction are minimized, the dynamic phenomenon during loading is weakened, and the failure mode changes from a mixed tensile-shear type to a tensile one. Due to the softening, lubrication, and water wedge effects in water-rock interactions, water content increases pore size, promotes crack development, and weakens micro-pore structures. Further damage of rocks in fractured and caved zones due to the water-rock interactions leads to an extra load on the adjoining coal and rock masses, which will increase the risk of dynamic disasters.

Keywords: acoustic emission; mechanical behavior; pore structure; sandstones; water content; water-rock interaction

1. Introduction

In recent years, intensive exploitation of coal resources in China has gradually transferred to west China and the coal mining depth has deepened significantly (the maximum exceeds 1500 m). Subsequently, dynamic disasters, such as coal or rock bursts, have occurred more frequently (Ranjith *et al*. 2017, Zhou *et al.* 2022). Aquifers overlying coal seams are commonly present when mining coal at depth (Wang *et al*. 2020a). The intrinsic mechanical properties of coal/rock and the extrinsic stress environment are the two dominant factors leading to coal/rock dynamic disasters (Li *et al*. 2019). Underground water significantly affects coal/rock properties as well as the stress field around the mining stope. A deep understanding of water-coal/rock interactions is important to ensure safe mining activities (Yuan *et al*. 2015).

Water content in coal and rock heavily depends on the internal microstructures and the soaking time (Wang 2020b, Liu *et al*. 2020). To obtain the mechanical parameters of different water-treated coals and rocks, a series of experiments, including uniaxial compression/tension tests, point-load tests, and triaxial compression tests, have been conducted (Pimienta *et al*. 2014, Hashiba and Fukui 2015, Masoumi *et al*. 2017, Kim *et al*. 2018, Zhang *et al*. 2020, He *et al*. 2021). The results show that the uniaxial compressive strength, uniaxial tensile strength, shear strength, Young's modulus, rigidity and brittleness, friction angle, plastic deformability, accumulation energy, and burst propensity all decrease with increasing water content, but that the Poisson's ratio increases. Moreover, acoustic emission (AE) tests on dry and saturated coal and rocks have been conducted and the results show that the AE activity of saturated samples in the loading process decreases while the crack initiation stress increases (Vishal *et al*. 2015). Crack development and failure modes of coal and rocks with different water contents have also been systematically investigated (Yao *et al*. 2020).

Coal and rocks in coal measure strata are porous media materials and their micro-pore structure significantly influences their physical and mechanical properties (Li *et al*. 2020). The detection of the response of the micro-pore structure to water, heat, liquid nitrogen, and other elements has increasingly been attracting extensive attention (Yang *et al*. 2017). A series of pore structure detection methods and equipment have been proposed and come into use, such as scanning electron microscopy (SEM) (Hadizadeh *et al.* 2010), micro-X-ray computed tomography (μ-CT) (Raynaud *et al*. 1989), transmission electron microscopy (TEM) (Janssen *et al*. 2011), mercury intrusion porosimetry (MIP) (Shapiro *et al*. 2017), nitrogen adsorption/desorption (NAD), CO2 adsorption/desorption (CAD), and nuclear magnetic resonance (NMR) (Davydov *et al*. 2018). Besides,

*Corresponding author, Ph.D.
E-mail: TB18020033B4@cumt.edu.cn
**Professor
E-mail: lmdou@126.com

ISSN: 2005-307X (Print), 2092-6219 (Online)

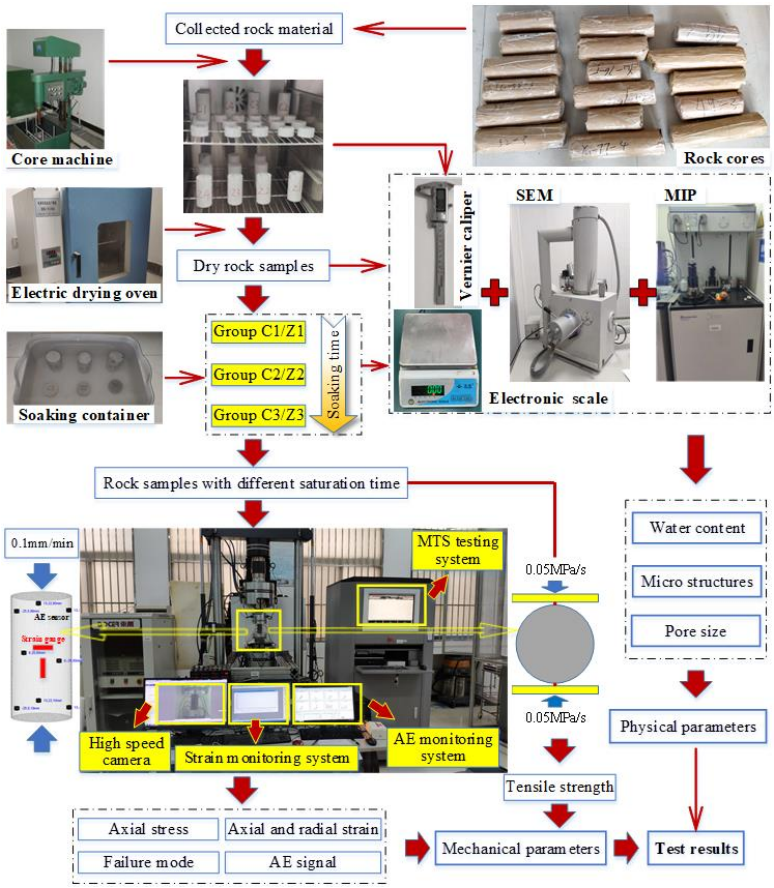

Fig. 1 Rock samples preparation method, test apparatus, and procedures

some numerical methods have gradually been used to study the pore structures evolution under different loading scheme (Zhang *et al*. 2021). These methods have been widely used and it has been shown that SEM is suitable for macropores, NAD for mesopores, CAD for micropores, and MIP for mesopores and macropores (Hodot 1966, Gaucher *et al*. 2011).

In underground coal mining engineering, many studies have focused on the effect of water on coal because water injection in coal is widely used to prevent coal bursts and other dynamic disasters (Xu *et al*. 2018). Some studies have focused on rocks concerning the effect of water for the safety of underground roadways or chambers by changing the macroscopically mechanical property (Li and Reddish 2004, Vásárhelyi and Ván 2006, Yang *et al*. 2021). However, the microscopic mechanism of underground water on rock property were rarely analyzed.

Comprehensive experimental data on the mechanical behavior of rocks subjected to different water treatments in coal measure strata and the micro mechanism are still limited. Besides, the effect of water-rock interactions on the stress field in surrounding rock of mining gob is significant for the monitoring and prevention of dynamic disasters, such as rockburst, coal and gas outbutst, etc. Therefore, further studies on rocks properties and microstructures subjected to different water treatments as well as its influence on the stress field in surround rock should be done.

In this study, sandstone samples were subjected to water treatments for different lengths of time. Then, uniaxial compression tests and tensile tests on different water-treated rock samples (i.e., dry, semi-saturated, and fully saturated) were conducted. The mechanical parameters, AE activities, dynamic phenomena (including rock splitting and sound), and failure patterns were analyzed. Furthermore, the micro-pore structures of different water-treated samples were tested using MIP and SEM. Finally, the water-rock interactions under load and their effect on rock properties were analyzed, the influence of water-rock interactions on the stress field in surrounding rock was discussed and some engineering recommendations for safe coal mining under aquifers were provided. The results of this study are expected to provide a deeper understanding of water-rock interactions as well as their effect on the mechanical behaviors of rocks and underground coal mining activities.

2. Experimental scheme

2.1 Rock samples preparation

The rock sample preparation method, test apparatus, and test procedure are shown in Fig. 1. Various rock cores with 85 mm diameter, including coarse sandstone and medium sandstone present between the 4# coal seam and the overlying Luohe aquifer, were derived from a 1000 m deep

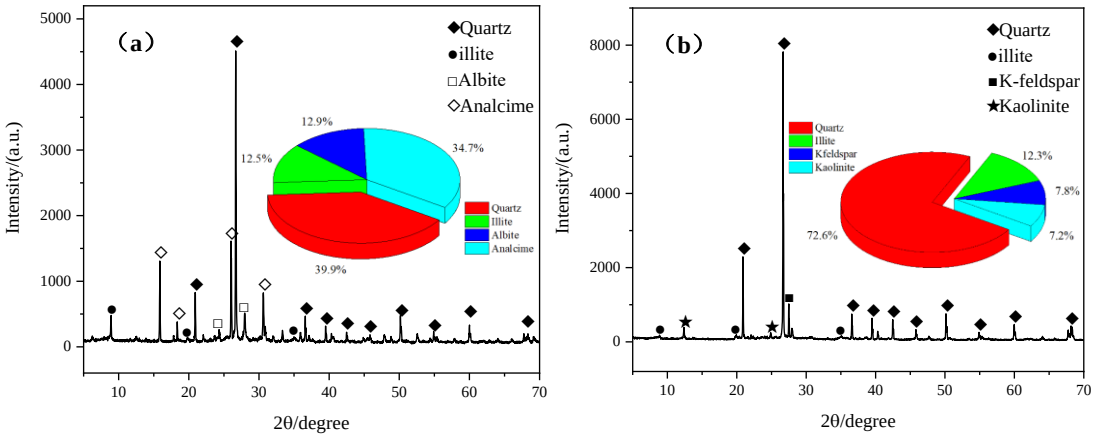

Fig. 2 Mineral compositions in the (a) coarse and (b) medium sandstone samples

Table 1 Physical and mechanical parameters of the rock samples determined by the uniaxial compression test

Rock lithology	Serial number	ρ_{dry} /kg·m^{-3}	$\omega_{natural}$ /%	p_{dry} /km·s^{-1}	T_w /h	ω_{real} /%	UCS /MPa	$\overline{UCS}$ /MPa	ε /%	E /GPa	μ
Coarse sandstone	C1-1	2715	1.12	1442		0	50.34		1.05	6.32	0.13
	C1-2	2750	1.08	1418	0	0	55.39	51.20	1.13	8.55	0.10
	C1-3	2718	1.15	1453		0	47.86		1.02	6.80	0.11
	C2-1	2732	1.14	1408		3.68	35.89		0.92	5.91	0.30
	C2-2	2722	1.11	1485	15	3.32	33.94	35.30	0.88	4.66	0.35
	C2-3	2745	1.15	1396		3.53	36.06		0.95	5.85	0.28
	C3-1	2726	1.07	1469		4.10	23.70		0.85	4.46	0.43
	C3-2	2748	1.13	1392	75	4.26	22.86	24.04	0.84	3.50	0.45
	C3-3	2718	1.10	1433		3.87	25.55		0.78	3.27	0.39
Medium sandstone	Z1-1	2853	0.80	1647		0	67.89		1.09	8.72	0.11
	Z1-2	2876	0.85	1683	0	0	70.92	68.08	1.16	8.80	0.09
	Z1-3	2848	0.79	1619		0	65.43		1.15	10.59	0.12
	Z2-1	2842	0.76	1662		3.25	57.43		0.99	7.45	0.13
	Z2-2	2869	0.80	1733	15	3.16	61.51	57.88	1.08	7.69	0.14
	Z2-3	2851	0.83	1625		3.51	54.69		0.92	6.57	0.11
	Z3-1	2850	0.81	1666		3.76	37.89		0.84	6.02	0.17
	Z3-2	2863	0.83	1708	75	3.72	34.50	37.90	0.91	5.80	0.19
	Z3-3	2872	0.75	1629		3.65	41.32		0.86	5.05	0.17

hole in the Gaojiapu Colliery, Shaanxi Province, China. 9 cylindrical coarse sandstone and 9 cylindrical medium sandstone samples of 50 mm diameter and 100 mm height, as well as equivalent coarse and medium rock samples of 50 mm diameter and 25 mm height were processed. Two ends of the samples were accurately ground. Then, the samples were randomly subdivided into three groups and there were 3 samples in each group. The coarse and medium sandstone samples for the uniaxial compression tests were named C1-1, C1-2,⋯C3-3 and Z1-1, Z1-2,⋯Z3-3, respectively. Those for the tensile tests were named C1-1-T, C1-2-T,⋯C3-3-T, and Z1-1-T, Z1-2-T,⋯Z3-3-T, respectively.

Fig. 2 shows the mineral composition in the sandstones used in the test by XRD analysis. It can be seen that some soluble minerals, such as Illite and Kaolinite, are included in the sandstone samples. In coarse and medium sandstone samples, the soluble minerals take up 12.5% and 19.5%, respectively. When interacting with water, these soluble minerals will dissolve and expand the existing raw fractures or form new ones, which will further change the mechanical properties of sandstone samples significantly.

2.2 Experimental apparatus

The MTS Landmark 375.50 system with a maximum load of 500 kN was used for both the uniaxial compression and the tension tests. During the uniaxial compression test, a PCI-II AE system with 8 AE sensors was used to monitor the AE signals. The sampling rate was 2 MHz and the threshold value was 40 db. TS3862 Static Resistance Strain Indicators with two digital strain gauges were used to acquire axial/circumferential strain. An Autopore IV 9500 mercury intrusion porosimeter (MIP) and a VEGA scanning electron microscope (SEM) were used to detect the micro-pore structures of the different water-treated samples. The MIP can identify pore sizes of 5 nm to 360 μm. The maximum mercury intruded pressure and the minimum extruded pressure are 228 MPa and 0.1 MPa, respectively.

2.3 Experimental methods

First, rock samples were dried for 24 hours in an electric drying oven at a temperature of 110℃. Before and after

Table 2 Physical and mechanical parameters of rock samples determined by the uniaxial tensile test

Rock lithology	Serial number	ρ_{dry}/kg·m^{-3}	$\omega_{natural}$/%	T_w/h	ω_{real}/%	UTS/MPa	$\overline{UTS}$/MPa
Coarse sandstone	C1-1-T	2722	1.15	0	0	4.56	4.46
	C1-2-T	2746	1.11		0	4.75	
	C1-3-T	2710	1.16		0	4.08	
	C2-1-T	2674	1.08	15	4.08	2.32	2.39
	C2-2-T	2755	1.09		3.85	2.65	
	C2-3-T	2659	1.15		4.11	2.19	
	C3-1-T	2730	1.10	75	4.47	1.04	1.12
	C3-2-T	2740	1.12		4.20	1.31	
	C3-3-T	2685	1.03		4.37	1.02	
Medium sandstone	Z1-1-T	2853	0.79	0	0	5.33	5.46
	Z1-2-T	2850	0.84		0	5.07	
	Z1-3-T	2908	0.70		0	5.98	
	Z2-1-T	2842	0.82	15	3.54	3.73	3.66
	Z2-2-T	2919	0.69		3.18	3.95	
	Z2-3-T	2855	0.80		3.61	3.31	
	Z3-1-T	2850	0.75	75	3.92	2.09	2.06
	Z3-2-T	2839	0.84		3.74	2.27	
	Z3-3-T	2862	0.80		4.20	1.83	

being oven-dried, the rock samples were weighed to calculate the natural water content. Then, the initial wave velocity of the dry rock samples was tested. Second, the rock samples in Group C3, Z3, C3-T, and Z3-T were immersed in water. During the immersion period, they were weighed regularly to determine the real water content. When the weight of the rock samples no longer changed, they were considered to have reached the saturation state. The water contents of the rock samples evolved similarly and those of C3-3, Z3-3, C3-3-T, and Z3-3-T are illustrated in Fig. 2. The water contents increase nonlinearly with the water intrusion time and finally converge to a certain value. Accordingly, the rock samples in Group C2, Z2, C2-T, and Z2-T were placed in water for 15 h for semi-saturation.

In most cases, rocks in underground engineering are under static load (Wang *et al*. 2018b). Therefore, displacement control was used to apply static load on the rock samples in uniaxial compression test and the loading rate was 0.1 mm/min (the corresponding strain rate was 1.6×10^{-5} s^{-1}) (Li *et al*. 2019). In the tension test, force control was used and the loading rate was 0.05 MPa/s. The test results are summarized in Table 1 and Table 2

Rock samples in this test were well processed and there were no macroscopic cracks or fissures on the surfaces. The dry densities (ρ_{dry}) of the coarse and medium sandstone samples are 2674 kg·m^{-3}-2750 kg·m^{-3} and 2839 kg·m^{-3}-2919 kg·m^{-3}, with standard deviations of 26.6 kg·m^{-3} and 21.7 kg·m^{-3}, respectively. Their natural water contents ($\omega_{natural}$) are 1.03%-1.16% and 0.69%-0.85%, with standard deviations of 0.035% and 0.046%, respectively. Their wave velocities (p_{dry}) are 1392 km/s-1485 km/s and 1619 km/s-1733 km/s, with standard deviations of 32.4 km/s and 38.9 km/s, respectively. The physical parameters presented above indicate the homogeneity of the rock samples and assure the reliability of the test results.

3. Test results

3.1 Water absorption laws

The water content (ω) of coal and rocks is always used to determine their water absorption (Wang *et al*. 2021) and it can be derived from Eq. (1)

$$\omega = \frac{m_w - m_d}{m_d} \times 100\% \tag{1}$$

where m_w and m_d are the wet and dry weights, respectively.

Fig. 3 depicts the water content variations of the coarse sandstone and medium sandstone samples. The water saturation process of the rock samples can be divided into three stages, i.e., stage I - this is the rapidly rising stage occurring in the first 12 h; stage II – this is the slowly rising stage and occurs from about 13 h to 45 h and; stage III – this is the phase approaching the stable stage and occurs from about after 45 h. In stage I, the water content in the rocks increases rapidly. Then, the water absorption rate gradually slows down and finally becomes approximately stable, which means the rocks are fully saturated.

From Fig. 3, it can be seen that the water contents of the coarse sandstone samples in both the uniaxial compression and tensile tests exceed those of the medium sandstone samples. In addition, the water contents of the D50 mm× H25 mm samples are generally higher than those of the D50 mm×H100 mm samples. This may be due to the effect of the sample size on the water absorption rate. Song *et al*. (2020) conducted water immersion experiments on samples of different sizes and showed that a smaller sample size enhanced the water absorption speed and increased the water content under the same water soaking time.

The relationship between the real water content and water intrusion time can be expressed by a logarithmic function as Eq. (2) (Yao *et al*. 2020, Tang *et al*. 2021)

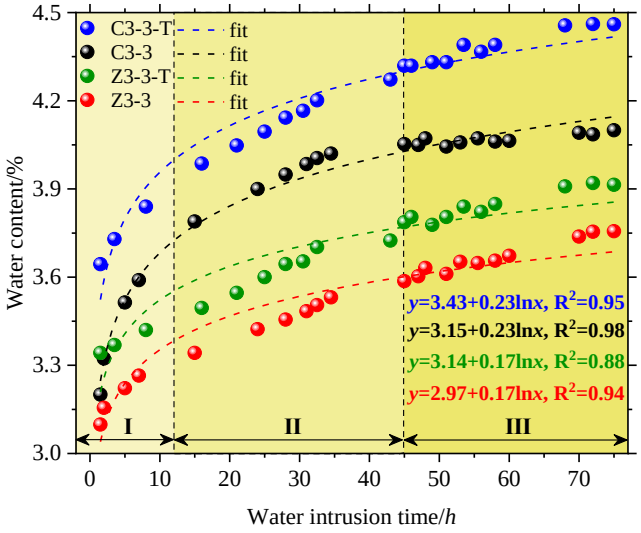

Fig. 3 Water content versus intrusion time of the rock samples

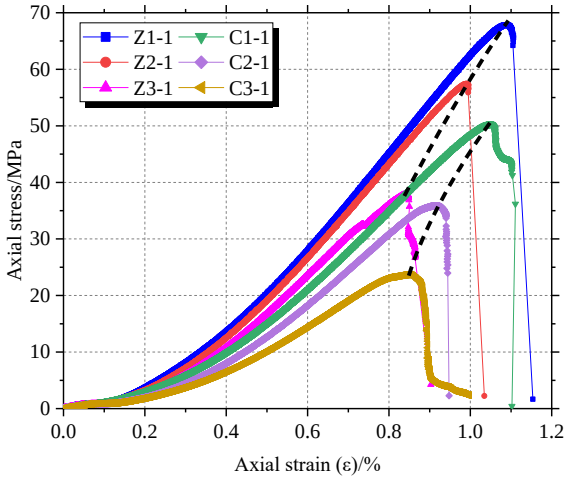

Fig. 4 Stress-strain curves of the tested rock samples

$$y = a + b\ln x \quad (2)$$

where y is the real water content (w_1); x is the water intrusion time, h; a, b are constants closely related to the physical and intrinsic properties of the rock samples.

It can be deduced that a is positively correlated with the sample size and negatively with the strength. However, b is more likely determined by the rock lithology. These constants will be further studied using various rocks through water soaking tests in the future.

3.2 Mechanical parameters

The typical stress-strain curves of different water-treated samples are shown in Fig. 4. With increasing load, the stress-strain curves all pass through the crack closure stage, the elastic deformation stage, the quasi-plastic deformation stage, and the post-peak stage (Mehdi *et al*. 2021). However, the stress-strain curves of different saturated samples differ significantly. Compared to the dry samples (group C1 and Z1), wet samples have lower peak stress, lower peak strain, lower Young's modulus, and minor stress drops; this is especially so for the fully saturated samples (group C3 and Z3). These explicit changes indicate that water treatment has a significant influence on the mechanical behavior of the rock both before and after the peak stress.

The mechanical strength parameters of the rock samples, i.e., the *UCS* and *UTS*, are illustrated in Fig. 5. It can be clearly seen that the *UCS* and *UTS* both decrease with the water soaking time. And both the *UCS* and *UTS* of the medium sandstone samples exceed those of the coarse sandstone samples. For the coarse sandstone samples, the mean *UCS* of the samples soaked for 15 h and 75 h declines by 31% and 53%, and the mean *UTS* declines by 46% and 75%, respectively, compared to the dry ones. For the medium sandstone samples, the mean *UCS* of the samples soaked for 15 h and 75 h declines by 15% and 44%, and the mean *UTS* declines by 33% and 62%, respectively, compared to the dry ones. Furthermore, the decreasing amplitudes of both the *UCS* and *UTS* of the coarse samples are obviously greater than those of the medium sandstone samples.

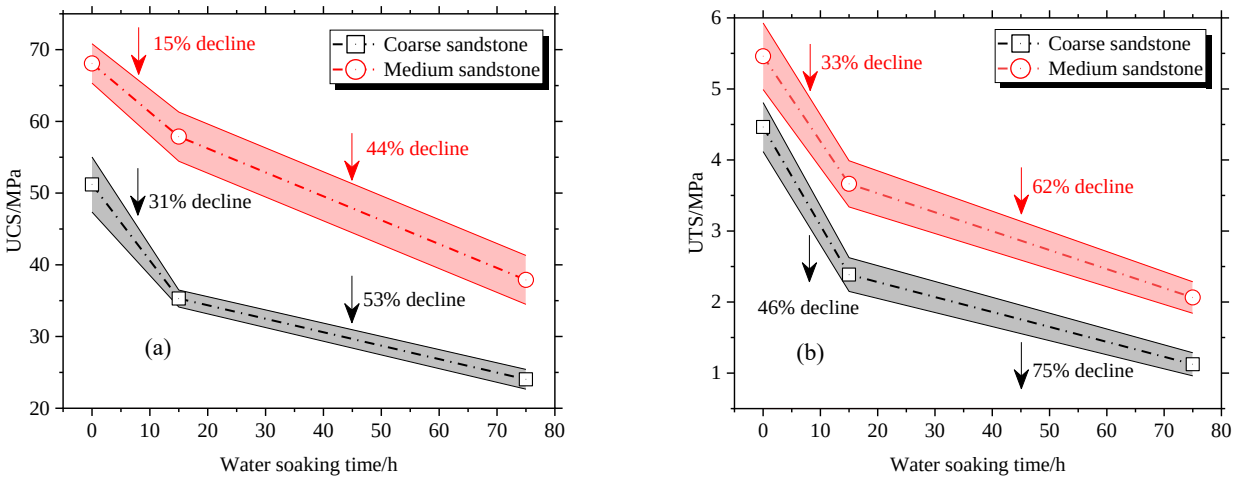

Fig. 5 (a) UCS and (b) UTS of the tested rock samples

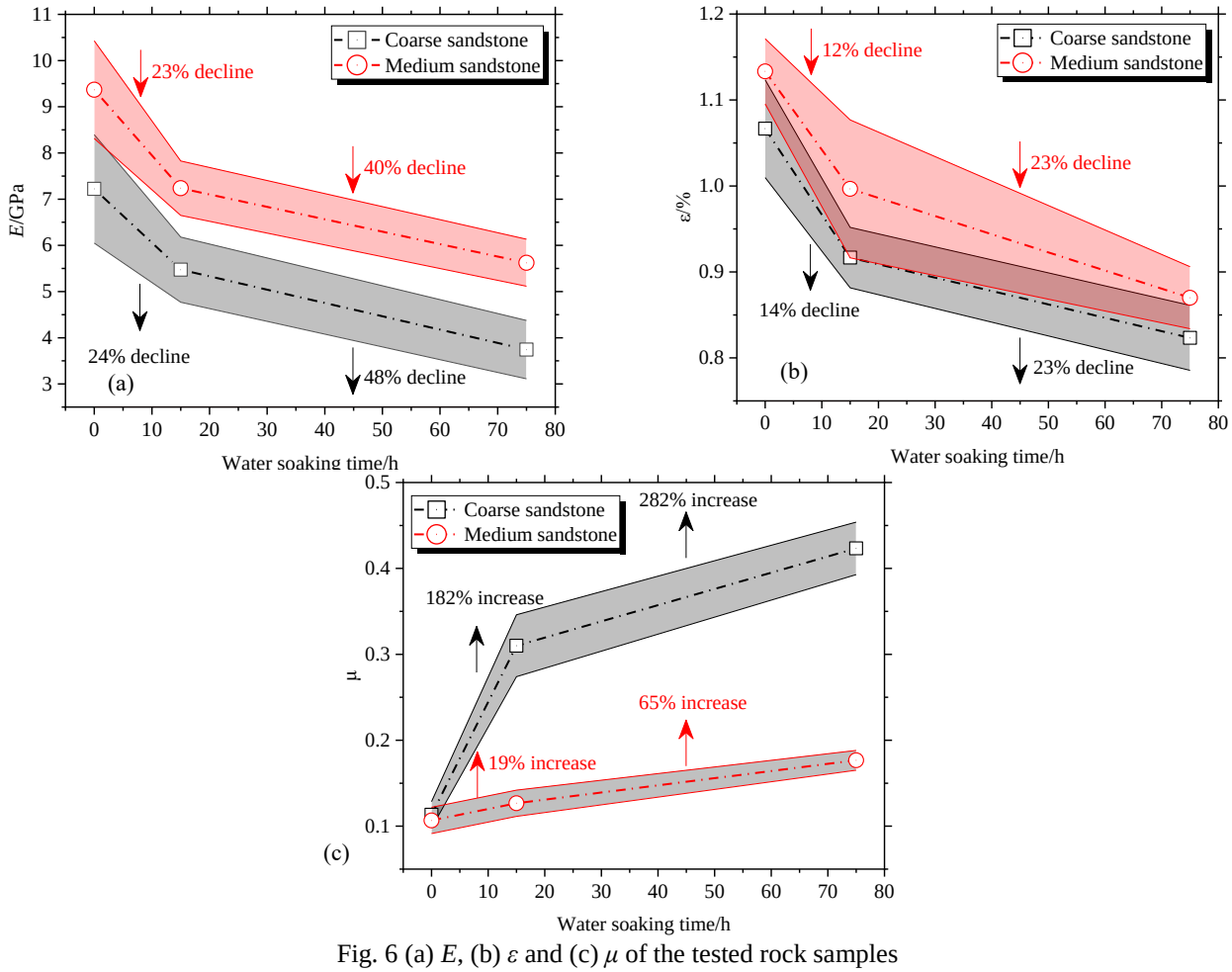

Fig. 6 (a) E, (b) ε and (c) μ of the tested rock samples

Fig. 6 shows the mechanical deformation parameters, i.e., E, ε, and μ. It can be seen that E and ε both decrease and μ increases with increasing water soaking time. E and ε of the medium sandstone samples with different soaking times are both higher than those of coarse sandstone samples, but μ changes contrarily. For coarse sandstone samples, the mean E of the samples soaked for 15 h and 75 h declines by 24% and 48%, and the mean ε declines by 14% and 23%, respectively, compared to the dry ones. The mean μ increases by 182% and 282%, respectively. For medium sandstone samples, the mean E of the samples soaked for 15 h and 75 h declines by 23% and 40%, and the mean ε declines by 12% and 23%, respectively, compared to the dry ones; The mean μ increases by 19% and 65%, respectively, compared to the dry ones. Besides, the decreasing amplitudes of E and ε of the coarse sandstone

Table 3 Accumulated counts and accumulated energy of the tested samples

Rock lithology	Serial number	T_w/h	Accumulated counts		Accumulated energy/aJ	
			test	average	test	average
Coarse sandstone	C1-1	0	367705	369887	4.5×10^7	4.2×10^7
	C1-2		422690		4.9×10^7	
	C1-3		319266		3.3×10^7	
	C2-1	15	28848	34337	6.6×10^6	6.6×10^6
	C2-2		31491		3.8×10^6	
	C2-3		42673		9.4×10^6	
	C3-1	75	30798	22931	5.3×10^6	3.5×10^6
	C3-2		15637		1.5×10^6	
	C3-3		22357		3.7×10^6	
Medium sandstone	Z1-1	0	373679	475261	6.8×10^7	7.3×10^7
	Z1-2		569710		9.5×10^7	
	Z1-3		482393		5.7×10^7	
	Z2-1	15	171838	178237	1.8×10^7	2.2×10^7
	Z2-2		138216		2.5×10^7	
	Z2-3		224657		2.3×10^7	
	Z3-1	75	59911	41816	2.0×10^7	1.4×10^7
	Z3-2		26973		0.6×10^7	
	Z3-3		38564		1.5×10^7	

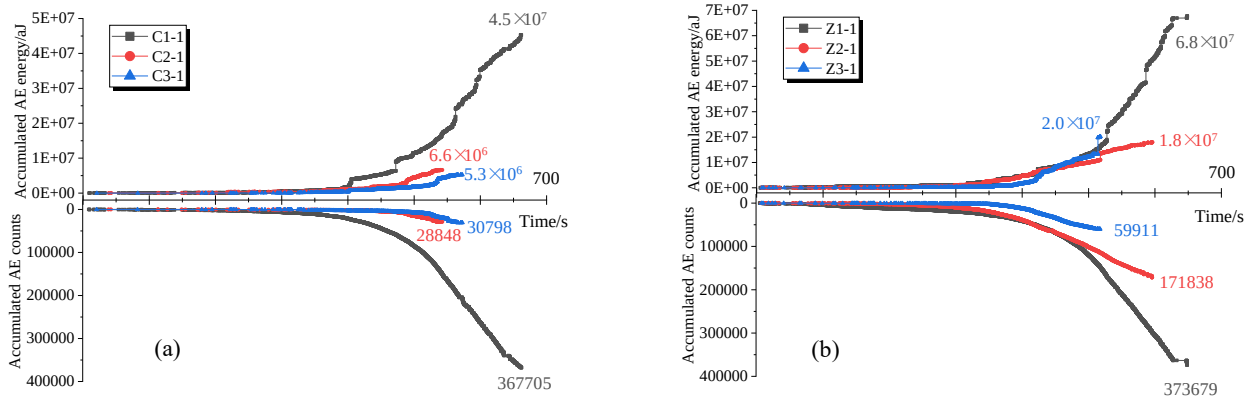

Fig. 7 AE activities of (a) coarse sandstone samples and (b) medium sandstone samples

samples are slightly higher than, or equivalent to, those of the medium sandstone samples. However, the increasing amplitudes of μ of the coarse sandstone samples significantly exceed those of the medium sandstone samples.

According to Figs. 5 and 6, the water content in the rock can weaken the rock strength significantly. The sensitivities to water treatment of the inferred parameters differ obviously. From high to low, they are μ, *UTS*, *UCS*, *E*, and ε, respectively. Rock lithology also influences the sensitivity of the mechanical parameters to water treatment and the mechanical parameter variation amplitudes of the coarse sandstone samples with lower strength are higher than those of the medium sandstone samples. This can be attributed to the different mineral compositions and micro-pore structures of the different rocks.

3.3 AE activities

AE activities can be used to mirror the crack development, propagation, and the crack transfixion to macroscopic failure in coal and rock samples (Vaneghi *et al.* 2020). The AE activities of some typical rock samples, including accumulated counts and accumulated energy, are given in Fig. 7.

AE activities of the tested rock samples evolve similarly. In the initial loading stage, the raw cracks and pores in the samples are compressed and some AE events with low energy may occur due to internal friction. Then, the samples come to the elastic deformation stage where scarcely any AE events occur. When the axial loading exceeds the elastic limit, the samples reach the plastic deformation stage and new cracks start to develop stably; meanwhile, the accumulated AE events increase steadily. When approaching the peak stress a large number of new cracks develop and interconnect to form minor fractures, which leads to a sharp and nonlinear increase in AE activities. With continued loading, the cracks and minor fractures eventually develop into macro fractures, leading to the thorough failure and a substantial release of elastic strain energy. In post-peak stage, some AE events with minor energy can also occur due to the friction along the macro fracture plane.

Table 3 presents the details of AE activities of the rock samples subjected to different water treatments. It can be

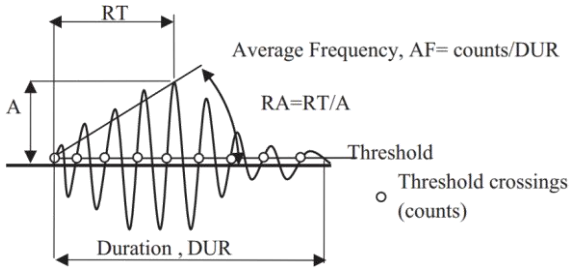

Fig. 8 Characteristic parameters of AE signals (Aggelis 2011)

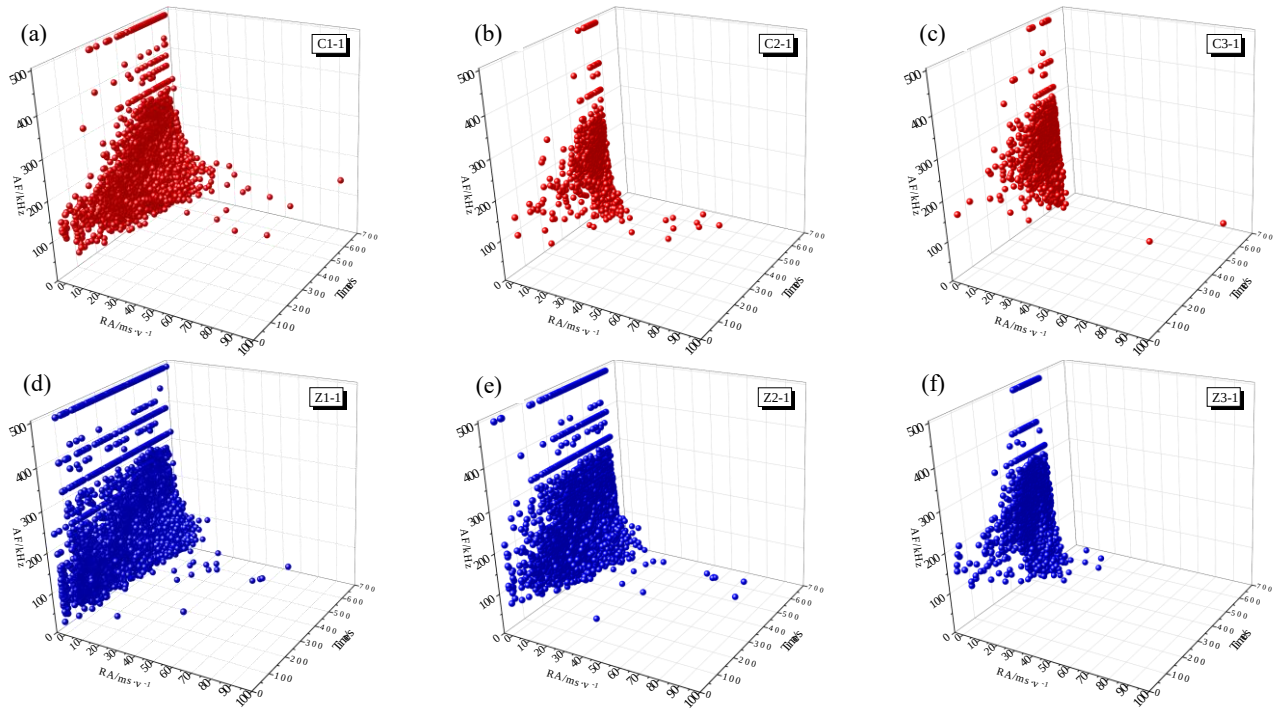

Fig. 9 RA-AF scatter plots of the uniaxial-loaded: (a)-(c) coarse sandstone samples and (d)-(f) medium sandstone samples

seen that AE activities of the water-treated samples, whether accumulated counts or accumulated energy, are weakened significantly. Taking the coarse sandstone samples for example, the average accumulated counts of the dry sample (0 h), the sample soaked for 15 h, and the sample soaked for 75 h are 369887, 34337, and 22931, respectively; the average accumulated energies are 4.2×10^7 aJ, 6.6×10^6 aJ, and 3.5×10^6 aJ, respectively. In addition, with the same soaking time, the AE activities of medium sandstone samples are stronger than those of coarse sandstone samples. However, the decreasing amplitudes of the AE activity of medium sandstone samples are less than those of coarse sandstone samples. Compared to the dry samples, the accumulated counts of fully saturated (75 h) coarse and medium sandstone samples decrease by 94% and 91%, and the accumulated energies decrease by 92% and 81%, respectively.

AE signals are characterized by a series of physical parameters as shown in Fig. 8 (Aggelis 2011). It is known that tensile cracks always lead to AE waveforms with short rise times and high frequencies; however, shear cracks are usually characterized by lower frequencies and longer rise times. That is, tensile cracks have high AF (count/duration time) and low RA (rise time/amplitude); on the contrary, shear cracks have low AF and RA (Ohno and Ohtsu 2010). AF and RA distributions can depict the influence of water content on crack development and failure modes.

Typical RA-AF-T scatter distributions of the coarse and medium sandstone samples are shown in Fig. 9. The RA and AF of the coarse and medium sandstone samples are 0-100 ms/v and 0-500 kHz, respectively. It can be seen that in the initial loading stage, only a few AE events with low RA and AF occur. With increasing loading, more AE events occur, and the maximum AF increases obviously; however, the maximum RA does not. When approaching the peak stress, the AE counts increase sharply, and their maximum AF reaches the peak and remains stable, while the maximum RA increases significantly. Moreover, AE events with high RA are usually accompanied by low AF. RA and AF evolutions in the test indicate that in the uniaxial loading process, the crack type changes from tensile cracks to tensile-shear cracks, especially in the dry rock samples.

For the different water-treated rock samples, the AE event amount decreases with increasing water soaking time and increasing water content. Furthermore, in the late loading stage, the maximum RA also decreases with

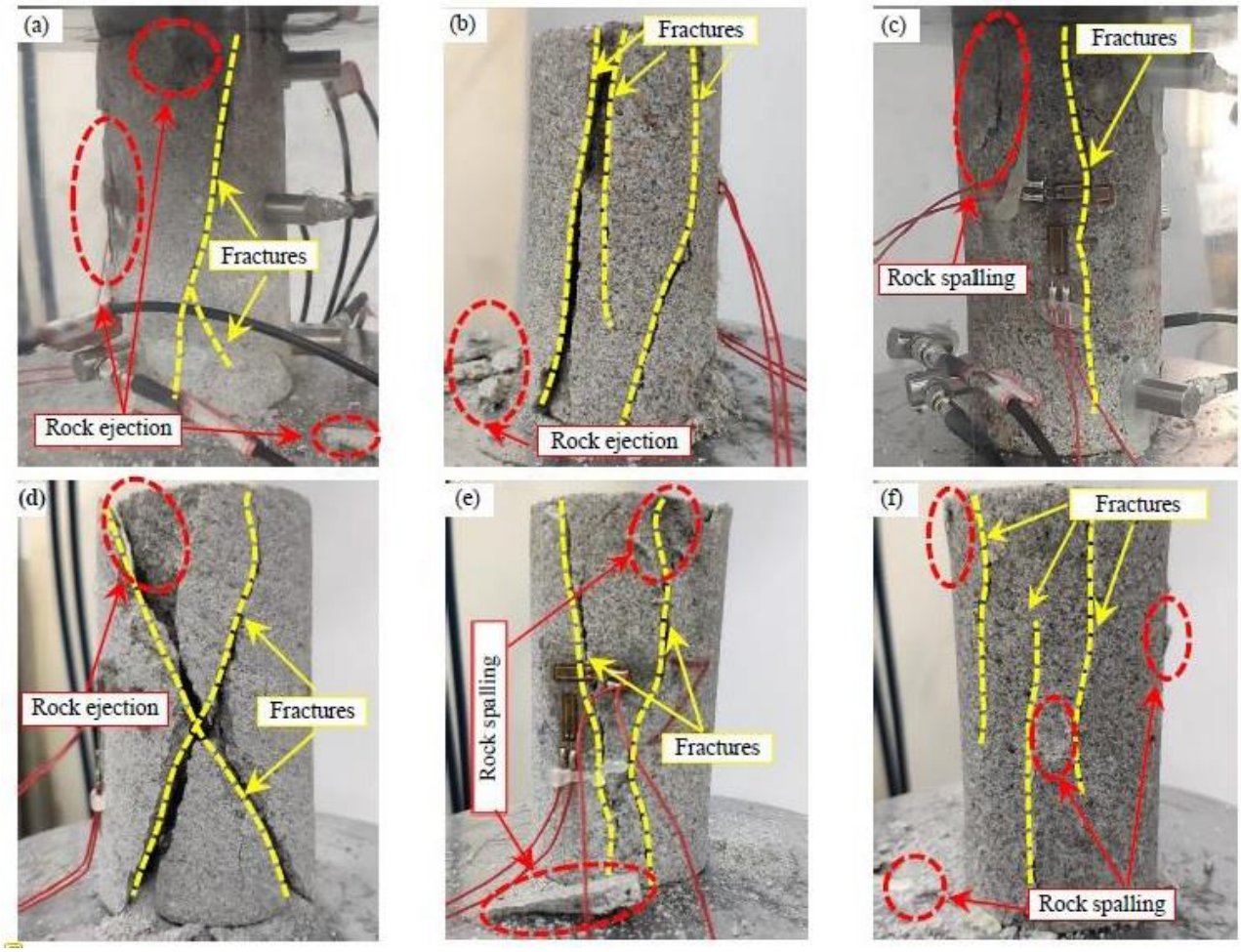

Fig. 10 Macro fractures and failure morphologies of the uniaxial-loaded: (a)-(c) coarse sandstone samples and (d)-(f) medium sandstone samples

increasing water soaking time and increasing water content, especially for the fully saturated samples (group C3 and group Z3). This indicates that the failure patterns of the rock samples during the water saturation process in the tests change from a tensile-shear type to a tensile one.

3.4 Failure features

Failure modes of rocks under uniaxial compression can be subdivided into three kinds based on their macro fracture morphology, i.e., tensile, shear, and mixed tensile-shear failure. In tensile failure, the macro fractures are almost parallel to the axial stress. In shear failure, the angle between the macro fractures and the axial stress is less than 45° or the failure plane is along a structural weakness. The mixed tensile-shear failure type is a combination of the two failures modes presented above, and the macro fracture morphology is always of an X shape. The failure modes of rocks are closely related to water content, joint inclination angle, porosity, and so on (Wang *et al.* 2018b). In fact, the failure of most rocks is due to joint tensile-shear fractures.

Some typical macro fractures and failure modes of the rock samples are illustrated in Fig. 10. It can be seen that the macro fractures and failure modes of different water-treated samples differ significantly. When the coarse sandstone samples are dry, only a macro fracture that is about 15° oblique to the loading direction is present. This indicates that the dry samples undergo shear failure. For the samples soaked in water for 15 h, simultaneous fractures occur parallel and oblique to the axial loading direction, which is a mixed tensile-shear failure. For the samples soaked in water for 75 h, the macro fractures are almost parallel to the loading direction which is a type of tensile failure. In addition, when dry and semi-saturated samples approach the peak stress, rock ejections are observed and the sudden failure leads to a violent noise and fierce shock. However, for fully saturated samples, the loading process is quite calm and only some rock spalling is observed on the surface.

Similar macro fractures and dynamic phenomena were observed during the uniaxial compression test of the medium sandstone samples. However, in contrast to the coarse sandstone samples, in the dry sample, the macro fractures were of X-shape, indicating a mixed tensile-shear failure. During the loading of both the dry and semi-saturated (15 h water treatment) samples, rock ejections occurred.

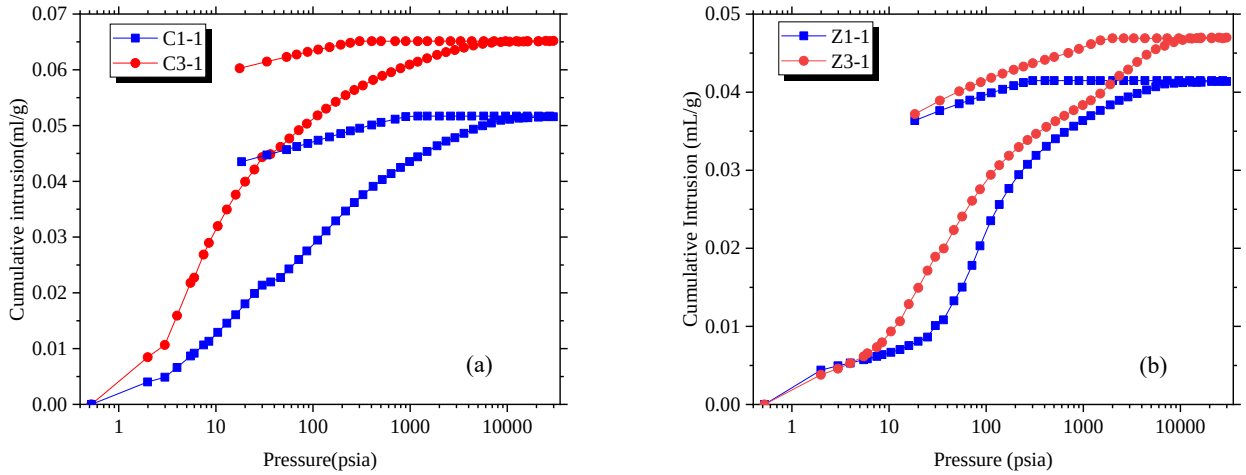

Fig. 11 Mercury penetration test results of the dry and fully saturated: (a) coarse and (b) medium sandstone samples

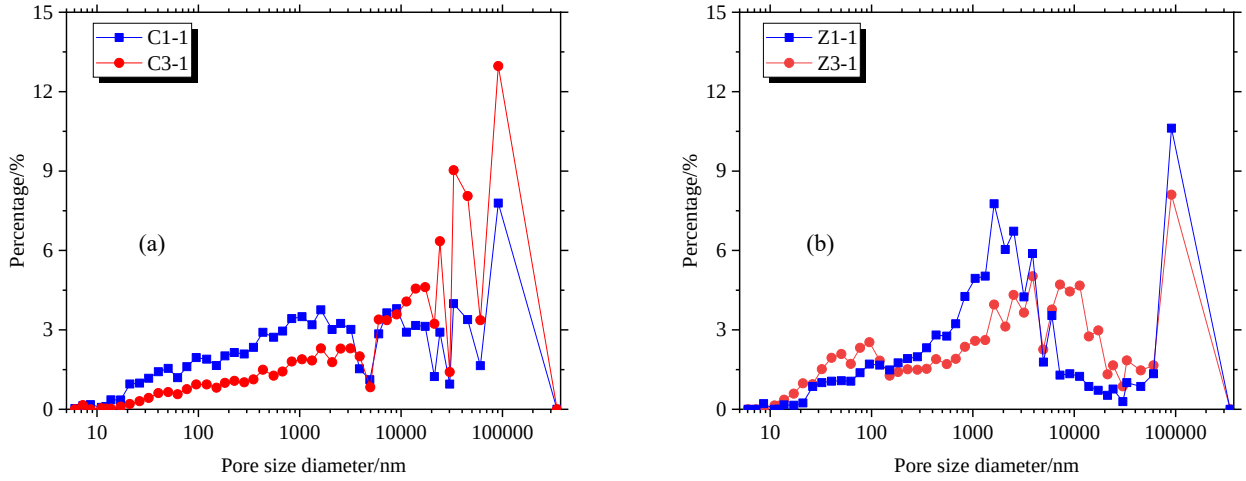

Fig. 12 Pore size distribution of the dry and fully saturated: (a) coarse and (b) medium sandstone samples

Therefore, water treatment can change the failure mode from shear or tensile-shear type to tensile one and weaken the dynamic phenomenon (including rock splitting intensity and the sounds) of rock samples significantly.

3.5 Pore structure features

The mechanical behavior of coal and rocks is closely related to their micro-pore structures. Mercury, for most rocks, is a nonwetting phase and it cannot permeate into pores without external pressure. It has been demonstrated that the external pressure is inversely proportional to the size of the mercury intruded pores (Gardner 1921), which can be expressed by Eq. (3)

$$P = \frac{-2\gamma cos\theta}{r} \quad (1)$$

where P is the mercury intrusion pressure, Pa; γ is the mercury surface tension, 485.0 N/m; θ is the contact angle, 140°; r is the pore size, cm.

In this test, the micro-pore structures of dry and fully saturated rock samples (C1-1, C3-1, Z1-1, and Z3-1) were tested using an AutoPore IV 9500 mercury porosimeter. The rock samples for the mercury intrusion test were obtained from the cylinder samples damaged in the axial compression test. They were crushed into a size of <1 cm and then dehydrated in an electric drying oven.

Fig. 11 shows the cumulative mercury intrusion curves with mercury pressure for the dry and fully saturated coarse and medium sandstone samples. It can be seen that the cumulative mercury intrusion for both the dry and the fully saturated samples increases with the capillary pressure and finally becomes stable. During the mercury extrusion progress, the curves first remain stable and then slowly decrease linearly when the capillary pressure is under a certain value. Obviously, there are hysteresis between the mercury ejection curves and the mercury injection curves, which indicates that there are substantial ink-bottle pores in the samples and that the connectivity between pores is poor.

In terms of water content in the rock, the mercury curves of the fully saturated samples, whether coarse sandstone or medium sandstone, exceed those of the dry samples. This indicates that water treatment can enlarge the pore size significantly.

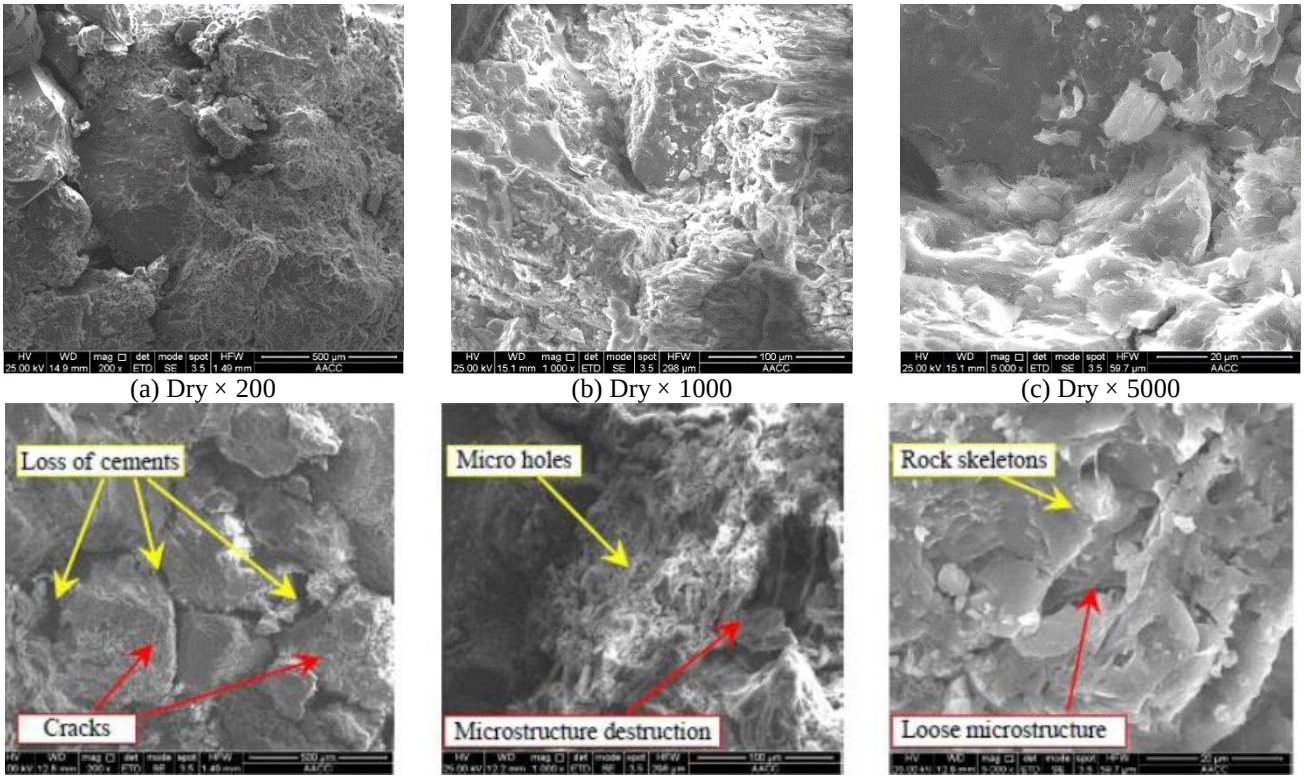

(a) Dry × 200 (b) Dry × 1000 (c) Dry × 5000

(d) Fully saturated × 200 (e) Fully saturated × 1000 (f) Fully saturated × 5000

Fig. 13 SEM results of (a)-(c): dry and (d)-(f): fully saturated coarse sandstone samples under various magnifications

Table 4 Pore structure parameters based on the MIP test results

No.s	Total Intrusion Volume (mL/g)	Porosity (%)	Average pore diameter (nm)	Percentage(%)			
				Micro pore (0-10 nm)	Transition pore (10-100 nm)	Medium pore (100-1000 nm)	Large pore (>1000 nm)
C1-1	0.052	12.10	250.1	0.35	11.73	24.14	63.78
C3-1	0.065	14.64	631.0	0.16	4.64	11.98	83.22
Z1-1	0.041	9.91	219.0	0.22	8.75	24.18	66.85
Z3-1	0.047	11.74	240.5	0.01	15.28	16.92	67.79

The pore size distributions of the tested samples are shown in Fig. 12 and the critical parameters of the pores are listed in Table 4. According to the Hodot classification method (Hodot 1966), pores with a size of 0-10 nm, 10-100 nm, 100-1000 nm, and >1000 nm are micro-pores, transition pores, medium pores, and large pores, respectively.

From Fig. 12 and Table 4, it can be seen that after water treatment, in the coarse samples, the large pore percentage increases significantly from 63.78% to 83.22%, and the percentages of micro-pores, transition pores, and medium pores all decrease simultaneously. In the medium samples, the percentages of the transition pores and large pores increase from 8.75% to 15.28% and from 66.85% to 67.79%, respectively. Correspondingly, the micro-pore and medium pore percentages decrease. In addition, after water saturation, the porosity and average pore diameter of the coarse sandstone samples increase from 12.10% to 14.64% and 250.1 nm to 631.0 nm, with increasing amplitudes of 21.0% and 152.3%, respectively. The porosity and average pore diameter of the medium sandstone samples increase from 9.91% to 11.74% and 219.0 nm to 240.5 nm, with increasing amplitudes of 18.5% and 9.8%, respectively.

The MIP test results indicate that water treatment can weaken micro-pore structures and increase the porosity and pore size. These changes then increase the permeability of the rock and lower its strength, which significantly affects its physical and mechanical behavior.

Microstructural characteristics were further tested using FEI Quanta^{TM} 250 scanning electron microscope (SEM). The test was conducted with a working current of 25 kV and a high vacuum + nonconductive mode. Cubic samples were derived from the surface parts of the failed samples and the average diameter of these samples was less than 1 cm. Prior to the test, the samples were oven-dried and overgilded.

Fig. 13 shows the SEM images of the dry and fully saturated coarse sandstone samples under 200, 500, and 2000 times of magnification, respectively. During water treatment, some physical and chemical reactions occur

Table 5 Mineral element percentage of dry and fully saturated coarse sandstone samples

Element	Percentage/%		
	Dry	Fully saturated	Variation
Oxygen (O)	57.28	49.86	-7.42
Silicon (Si)	15.20	21.4	6.20
Aluminium (Al)	3.43	11.67	8.24
Potassium (K)	1.35	0.19	-1.16
Sodium (Na)	0.68	8.81	8.13
Carbon (C)	5.80	7.38	1.58
Iron (Fe)	1.05	0.3	-0.75
Magnesium (Mg)	0.43	0.26	-0.17
Sulfur (S)	5.92	0.08	-5.84
Titanium (Ti)	0.33	0.04	-0.29
Calcium (Ca)	8.52	0.00	-8.52

because of long-term hydration, which leads to some microdefects in the microstructures (micro-cracks, micro-holes, etc.). Under 200 times magnification, the surface and internal structure of the dry samples have good integrity, the rock particles are tightly cemented, and no micro-cracks exist on the surface, as shown in Fig. 13(a). However, after water treatment, most of the cement among the rock particles disappear, the cementation is weakened, the rock particles are separated, and more pore-connecting cracks form, as shown in Fig. 13(d). Moreover, several intraparticle cracks are clearly observed which may be due to the inhomogeneous expansion of rock particles and the concentrated stress in adjacent particles. Under 1000 times magnification, the surface of the dry sample is quite smooth and there are clear striations and some bright-colored mineral grains, as shown in Fig. 13(b). However, in the fully saturated samples, the surface is rough, and substantial micro holes and some microstructure destructions are observed, as shown in Fig. 13(e). Under 5000 times magnification, the microstructures of the dry samples are intact, but after water treatment, only rock skeletons are left and some soluble minerals are dissolved in water or independent grains are swept away, leading to a loose microstructure as shown in Figs. 13(c) and (f).

To obtain the distribution and content of the mineral elements of the samples subject to different water treatments, energy spectrum analysis (ESD) was performed with the FEI QuantaTM 250 SEM presented in section 3.5.

The ESD results of the dry and fully saturated coarse sandstone samples (C1-1 and C3-1) under 5000 times magnification are listed in Table 5. It can be seen that after water treatment, some mineral element percentages, including Potassium (K), Iron (Fe), Magnesium (Mg), Sulfur (S), Titanium (Ti), and Calcium (Ca), decrease significantly. This indicates that during the process of water saturation, some mineral compounds (such as $CaCO_3$) are dissolved in water, which leads to the disappearance of the cementation material, as shown in Fig. 13(d), and the formation of micro-holes and loose microstructures as shown in Fig. 13(e) and Fig. 13(f), respectively.

4. Discussion

4.1 Water-rock interactions

According to the 1000 m deep drilling hole exploration report in Gaojiapu colliery, the coarse sandstone and medium sandstone samples are purplish red and brownish red, respectively. The main mineral components of the sandstones are quartz, feldspar, clastic, and other dark-colored clay minerals. After water treatment, the presence of water in rocks can bring about microstructural changes, including the dissolution of some mineral substances, the formation of micro-cracks, and the expansion of internal pores and particles. In terms of the physical-mechanical parameters and microstructural changes discussed above, the following water-rock interactions can be concluded.

1) Softening effect

There are substantial pore-filling cemented materials and structures in rocks. When immersed in water, a series of physical and chemical reactions occur. The cementing substances between particles, and especially the clay minerals (in Fig. 2), dissolve in the water. The typical chemical reaction can be expressed as Eq. (4) and Fig. 14 (Wang *et al*. 2021). Consequently, rock particles are separated, and more pore-connecting cracks form. Moreover, the calcite crystal particles expand in the water, which weakens the strength of the rock and leads to the formation of new interior cracks between particles, as shown in Fig. 14. The corrosion of the cement material between particles and the formation of new cracks increases the porosity and permeability and softens the rock significantly.

$$CaCO_3 + H_2O + CO_2 \rightarrow Ca(HCO3)_2 \quad (4)$$

2) Lubrication effect

Water seeps into rocks through the original pores and cracks and then exists mainly in two forms, i.e., adsorbed water and free water (Yu *et al*. 2013). The adsorbed water is fixed on the rock particles, while the free water is reserved in the initial and newborn cracks and discontinuities. When loaded, the cracks slip along the crack plane. The adsorbed

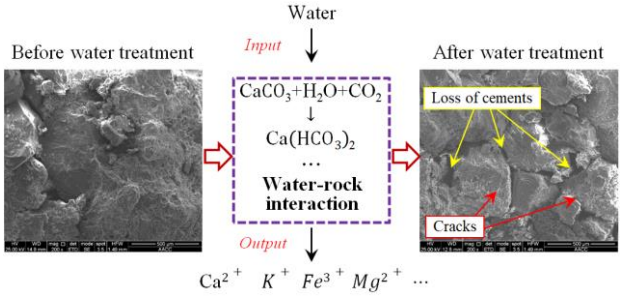

Fig. 14 Softening effect of water in rocks

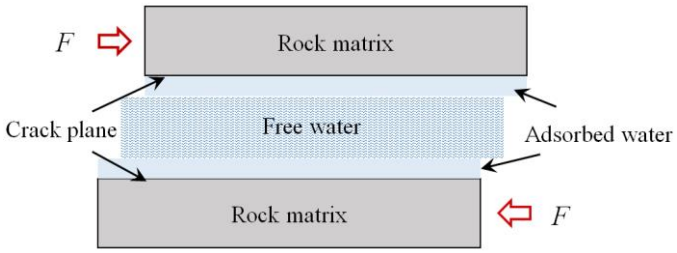

Fig. 15 Lubrication effect of water in rocks

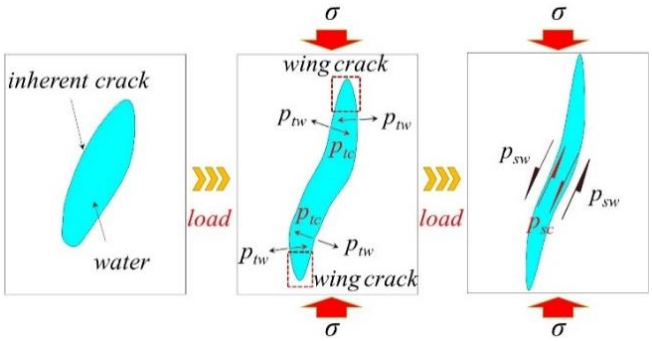

Fig. 16 Water wedge effect on crack development

water reduces the frictional resistance and the crack slides and fails under low external loads (Song *et al*. 2020), as shown in Fig. 15. The bearing capacity of the rock is consequently further weakened.

3) Water wedge effect

As shown in Fig. 16, when water-treated samples are loaded, the internal pores and cracks get condensed, and consequently, the water pressure (p_{tw}) increases; moreover, the softening effect of water on the mineral particles and the microstructural damage both cause the critical crack initiation stress (p_{tc}) to decrease. A higher p_{tw} and lower p_{tc} both act on the tips of the inherent cracks and promote the development and expansion of tensile cracks (Zhou *et al*. 2020a). These newborn cracks connect and form macro fractures. Meanwhile, when the shear stress (p_{sw}) along the macro fracture plane exceeds the critical shear stress (p_{sc}), sliding will occur along the macro fracture and even lead to collapse of the rock. It should be noted that due to the softening effect of water and the lubrication effect, the p_{sc} decreases, and consequently, macro fractures fail at a low p_{sw}.

4.2 Effect of water on rock properties

During the water saturation process, water seeps into rocks via pre-existing cracks. Coarse and medium sandstones are typical sedimentary rocks with substantial cementation material (Wang *et al*. 2021). Due to the softening effect of water, the cohesion between rock particles is reduced, the rock particles including feldspar expand and soften, and micro-crack development is boosted (Kuznetcov *et al*. 2018, Wang *et al*. 2018a). These microstructural changes increase the rock's porosity, permeability, and compressibility, leading to a decrease in E and an increase in μ as shown in Fig. 6. During uniaxial compression, due to the lubrication effect and the water wedge effect, sliding will occur along micro-cracks at lower stresses and then these micro-cracks interact to form macro fractures. Crack development in rocks exposed to water, on the one hand, weakens the bearing capacity of the rocks significantly, leading to a decrease in the *UCS* and *UTS* as shown in Fig. 5; on the other hand, it lowers the critical stress required for crack initiation, expansion, and failure as well as the dynamic phenomenon, leading to the weak AE

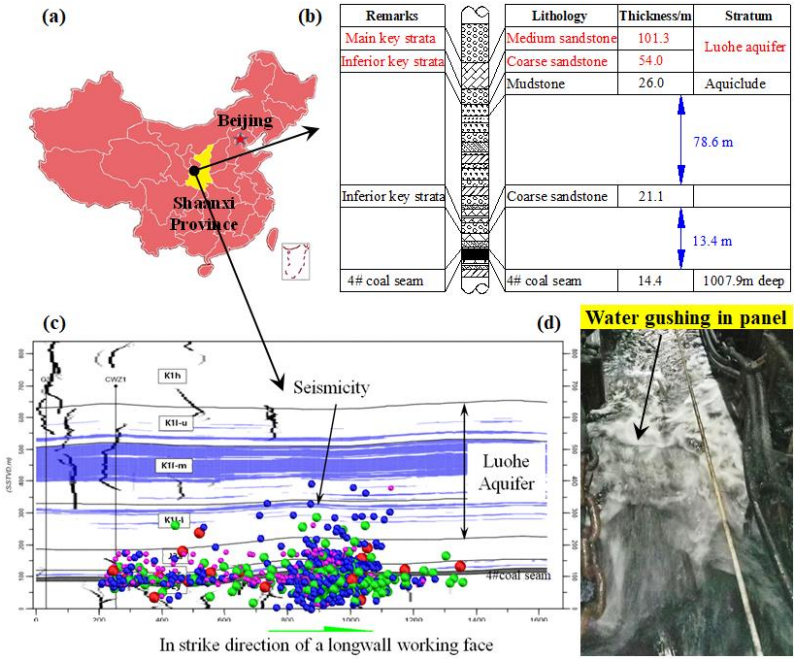

Fig. 17 Stratigraphic column, mining-induced fractures and water gushing of the Gaojiapu colliery in China

activities shown in Fig. 7 and the quiet loading process in Fig. 10. In addition, because of the water wedge effect, the percentage of tensile cracks in the late loading stages increases. On the contrary, the lubrication effect causes the micro-cracks or macro fractures to collapse at a lower stress and decreases the elastic energy released by shear failure. This can account for the RA-AF scatter distribution in Fig. 9. The tensile test results indicate that when the coarse and medium sandstone samples are fully saturated, their *UTS* declines by 75% and 62%, respectively. Saturated rocks are more prone to tensile failure.

According to the Mohr-Coulomb failure criterion, the angle (β) between the principal stress and the macro failure plane can be expressed by Eq. (5).

$$\beta = \frac{\pi}{4} + \frac{\varphi}{2} \tag{5}$$

where φ is the internal friction angle of rocks.

The uniaxial compression and tension test results show that water content can weaken rock strength significantly. φ, which is one of the primary strength parameters of rocks, decreases with increasing water content (Xiong *et al*. 2011, Wang *et al*. 2018a). Likewise, when the water content in rocks increases, β decreases. This matches the macro fracture distribution in Fig. 10 well. The AE activities, macro fracture distribution, dynamic phenomenon, and the water-rock interaction at the microscale analyzed above indicate that increasing the water content changes the failure form of the rock from a shear or tensile-shear type to a tensile one.

4.3 Guidance for safe mining activity

The Gaojiapu colliery in Shaanxi province, China has suffered from rock bursts for about 7 years since coal entry development (Zhou *et al*. 2020b). The stratigraphic column is illustrated in Fig. 17.

The coal seam is about 1000 m deep and the average thickness is 11 m. There is a super-thick Luohe confined aquifer about 150 m above the coal seam. Based on the key strata theory (Sun *et al*. 2019), the coarse sandstone and the medium sandstone in the Luohe aquifer are inferior key stratum and main key stratum, respectively. During coal mining of the longwall working face, the caving height is 6.0-9.0 m. Underground microseismic monitoring results indicate that mining-induced fractures have reached the lower part of the Luohe aquifer (main key strata). Ground subsidence results show that the maximum subsidence is 0.5 m and that the main key strata in the Luohe aquifer are stable. The maximum water inflow can reach up to 800 m^3/h in the working face.

Generally, when coal is extracted out from a longwall working face, the overlying strata, in terms of the deformation characteristics, can be subdivided into three zones, i.e., the caving zone, the fractured zone, and the continuous deformation zone, as shown in Fig. 18.

The test results in this study show that after water treatment, the mechanical strength and bearing capacity of rocks are reduced and that their compressibility and deformability are enhanced. When the confined water from the Luohe aquifer enters the fractured and caved zones, a series of water-rock interactions under load occurs. This can exert significant influence on the physical and mechanical properties of the broken or fractured rocks (Wang *et al*. 2018b), leading to the further damage of the rocks and a decrease in the support for the overlying strata. This causes the excess load to be transferred to the deeper coal and rock mass, and the mining-induced stress field in both the strike and inclination directions is redistributed, as illustrated in Fig. 18(a). The abutment stress distribution can change

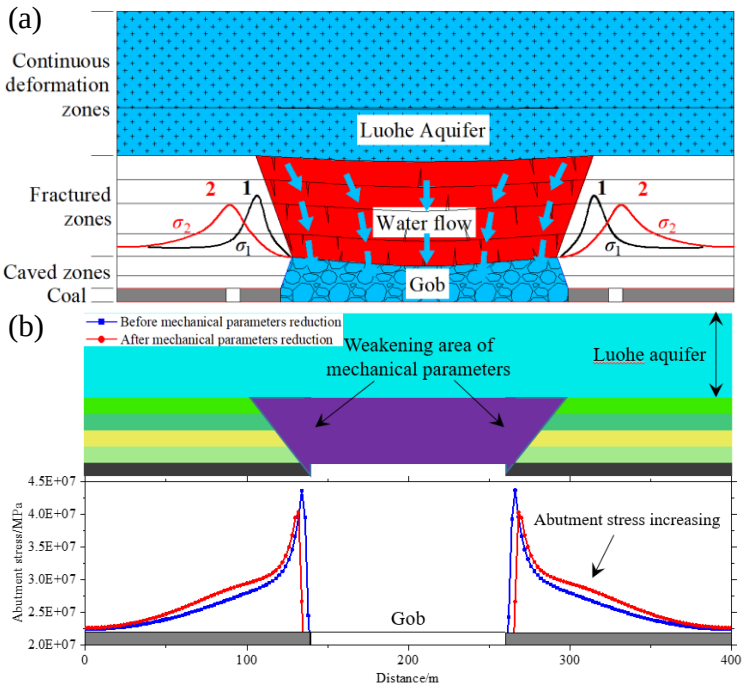

Fig. 18 Mining-induced stress field concerning water weakening effect on rock strength

from curve 1 to curve 2, leading to a lower peak stress and a greater influence range. Moreover, the peak stress is farther from the working face. An extra load will be exerted on the advanced area in the strike direction or the adjoining working faces in the inclination direction, which will increase the risks of dynamic disasters, such as coal bursts or coal-gas outbursts (Li *et al*. 2019). And this is also verified by the numerical simulation results in Fig. 18(b), where the mechanical parameters, including elastic modulus, cohesion and tensile strength, are reduced by 20%. Therefore, more attention, including monitoring and pressure-relief measures, should be paid to the advanced area in the strike direction or the adjoining working faces in the inclination direction. In addition, curtain grouting blocking (Seunghwan 2017) can be adopted to minimize the influence of the overlying aquifer on coal mining.

5. Conclusions

Water absorption of two sandstones and the mechanical properties of different water-treated samples were investigated in this study. AE monitoring and micro pore structure detection were carried out. Mechanical parameters, AE activities, failure mode, and pore structures of different water-treated sandstone samples were analyzed. The following conclusions are obtained.

- The water saturation process of rocks can be subdivided into three stages: the rapidly rising stage, the slowly rising stage, and the stable stage. The water content versus intrusion time can be expressed as a logarithmic function. Water absorption of rocks depends on the pore structures and sample size of the rock.
- Water content can significantly weaken rock strength. When fully saturated, the *UCS* of coarse and medium sandstone samples decrease by 53% and 44%, and the *UTS* decrease by 75% and 62%, respectively. The sensitivities to water treatment of the μ, *UTS*, *UCS*, *E*, and ε decrease systematically. For different rocks, the sensitivity of mechanical parameters to water treatment is inversely proportional to the rock strength.
- After water treatment, AE activities and the shear crack percentage are reduced, the angles between macro fractures and the axial loading direction are minimized, the dynamic phenomenon is weakened, and the failure mode changes from a tensile-shear type to a tensile one.
- Water content can increase the pore size, promote crack development, and weaken rock micropore structures. The water-rock interactions under load are mainly the softening effect, the lubrication effect, and the water wedge effect.
- In coal mines similar to the Gaojiapu colliery, the inflow of water will lead to further damage of rocks in the fractured and caved zones and a decrease in the support for the overlying strata. The extra load will be transferred to the adjoining coal and rock mass, which will increase the risks of dynamic disasters. More monitoring and pressure-relief measures should be adopted to guarantee the safety of coal mining.

Acknowledgments

This work was supported by National Natural Science Foundation of China [grant number 51874292; 51934007; 52004004] and Postgraduate Research & Practice

Innovation Program of Jiangsu Province [grant number KYCX21_2341].

References

Aggelis, D.G. (2011), "Classification of cracking mode in concrete by acoustic emission parameters", *Mech. Res. Commun.*, **38**(3), 153-157. https://doi.org/10.1016/j.mechrescom.2011.03.007.

Davydov, V.V., Myazin, N.S., Dudkin, V.I. and Velichko, E.N. (2018), "Investigation of condensed media in weak fields by the method of nuclear magnetic resonance", *Russian Phys. J.*, **61**(1), 162-168. https://doi.org/10.1007/s11182-018-1380-z.

Gardner, W. (1921), "Note on the dynamics of capillary flow", *Phys. Rev.*, **18**(3), 206-209. https://doi.org/10.1103/PhysRev.18.206.

Gaucher, E.C., Défossez, P.D.C., Bizi, M., Bonijoly, D., Disnar, J.R., Défarge, F.L., Garnier, C., Finqueneisel, G., Zimny, T., Grgic, D., Pokryszka, Z., Lafortune, S. and Gilbert, S.V. (2011), "Coal laboratory characterisation for CO_2 geological storage", *Energy Procedia*, **4**(1), 3147-3154. https://doi.org/10.1016/j.egypro.2011.02.229.

Hadizadeh, J., Sehhati, R. and Tullis, T. (2010), "Porosity and particle shape changes leading to shear localization in small-displacement faults", *J. Struct. Geol.*, **32**(11), 1712-1720. https://doi.org/10.1016/j.jsg.2010.09.010.

Hashiba, K. and Fukui, K. (2015), "Effect of water on the deformation and failure of rock in uniaxial tension", *Rock Mech. Rock Eng.*, **48**(5), 1751-1761. https://doi.org/10.1007/s00603-014-0674-x.

He, M.M., Zhang, Z.Q., Zhu, J.W. and Li, N. (2021), "Correlation between the constant m_i of Hoek-Brown criterion and porosity of intact rock", *Rock Mech. Rock Eng.*, **55**(2), 923-936. https://doi.org/10.1007/s00603-021-02718-2.

Hodot, B.B. (1966), *Coal and gas outburst*, China Industrial Press, Beijing, China.

Janssen, C., Wirth, R., Reinicke, A., Rybacki, E., Naumann, R., Wenk, H.R. and Dresen, G. (2011), "Nanoscale porosity in SAFOD core samples (San Andreas Fault)", *Earth Planetary Sci. Lett.*, **301**(1-2), 179-189. https://doi.org/10.1016/j.epsl.2010.10.040.

Kharghani, M., Goshtasbi, K., Nikkah, M. and Ahangari, K. (2021), "Investigation of the Kaiser effect in anisotropic rocks with different angles by acoustic emission method", *Appl. Acoust.*, **175**(4), 107831. https://doi.org/10.1016/j.apacoust.2020.107831.

Kim, E., Garcia, A. and Changani, H. (2018), "Fragmentation and energy absorption characteristics of Red, Berea and Buff sandstones based on different loading rates and water contents", *Geomech. Eng.*, **4**(2), 151-159. https://doi.org/10.12989/gae.2018.14.2.151.

Kuznetcov, N., Fedotova, I. and Pak, A. (2018), "Study of physical-mechanical properties of hard rocks under water-saturated conditions", *Proceedings of the International European Rock Mechanics Symposium (EUROCK)*, Saint Petersburg, RUSSIA, May.

Li, Y., Yang, J.H., Pan, Z.J. and Tong, W.S. (2020), "Nanoscale pore structure and mechanical property analysis of coal: An insight combining AFM and SEM images", *Fuel*, **260**, 116352. https://doi.org/10.1016/j.fuel.2019.116352.

Li, Z.L., He, X.Q., Dou, L.M., Song, D.Z., Wang, G.F. and Xu, X.L. (2019), "Investigating the mechanism and prevention of coal mine dynamic disasters by using dynamic cyclic loading tests", *Saf. Sci.*, **115**, 215-228. https://doi.org/10.1016/j.ssci.2019.02.011.

Liu, H.L., Zhu, W.C., Yu, Y.J., Xu, T., Li, R.F. and Liu, X.G. (2020), "Effect of water imbibition on uniaxial compression strength of sandstone", *Int. J. Rock Mech. Min. Sci.*, **127**:104200. https://doi.org/10.1016/j.ijrmms.2019.104200.

Masoumi, H., Horne, J. and Timms, W. (2017), "Establishing empirical relationships for the effects of water content on the mechanical behavior of gosford sandstone", *Rock Mech. Rock Eng.*, **50**, 2235-2242. https://doi.org/10.1007/s00603-017-1243-x.

Ohno, K. and Ohtsu, M. (2010), "Crack classification in concrete based on acoustic emission", *Constr. Build. Mater.*, **24**(12), 2339-2346. https://doi.org/10.1016/j.conbuildmat.2010.05.004.

Pimienta, L., Fortin, J. and Guéguen, Y. (2014), "Investigation of elastic weakening in limestone and sandstone samples from moisture adsorption", *Geophys. J. Int.*, **199**(1), 335-347. https://doi.org/10.1093/gji/ggu257.

Ranjith, P.G., Zhao, J., Ju, M.H., De Silva, R.V.S., Rathnaweera, T.D. and Bandara, A.K.M.S. (2017), "Opportunities and challenges in deep mining: A brief review", *Eng.*, **3**(4), 546-551. https://doi.org/10.1016/J.ENG.2017.04.024.

Raynaud, S, Fabre, D, Mazerolle, F., Geraud, Y. and Latière, H.J. (1989), "Analysis of the internal structure of rocks and characterization of mechanical deformation by a non-destructive method: X-ray tomodensitometry", *Tectonophysics*, **159**(1-2), 149-159. https://doi.org/10.1016/0040-1951(89)90176-5.

Seunghwan, K., Rim Heuidae, D. and Seongmin Y. (2017), "A Study on the impermeable effect by grouting in the subsea tunnel", *J. Korean Geo-Environ. Soc.*, **18**(6), 5-19. https://doi.org/10.14481/jkges.2017.18.6.5.

Shapiro, A.M., Evans, C.E. and Hayes, E.C. (2017), "Porosity and pore size distribution in a sedimentary rock: Implications for the distribution of chlorinated solvents", *J. Contaminant Hydrology*, **203**, 70-84. https://doi.org/10.1016/j.jconhyd.2017.06.006.

Song, H.H., Zhao, Y.X., Jiang, Y.D. and Du, W.S. (2020), "Experimental investigation on the tensile strength of coal: consideration of the specimen size and water content", *Energies*, **13**(24), 6585. https://doi.org/10.3390/en13246585.

Sun, Y.J., Zuo, J.P., Karakus, M. and Wang, J.T. (2019), "Investigation of movement and damage of integral overburden during shallow coal seam mining", *Int. J. Rock Mech. Min. Sci.*, **117**, 63-75. https://doi.org/10.1016/j.ijrmms.2019.03.019.

Tang, C.J., Yao, Q.L., Xu, Q., Shan, C.H., Xu, J.M., Han, H. and Guo, H.T. (2021), "Mechanical failure modes and fractal characteristics of coal samples under repeated drying–Saturation conditions", *Nat. Resour. Res.*, **2021**, 1-18. https://doi.org/10.1007/s11053-021-09905-6.

Vaneghi, R.G., Thoeni, K., Dyskin, A.V., Sharifzadeh, M. and Sarmadivaleh, M. (2020), "Strength and damage response of sandstone and granodiorite under different loading conditions of multistage uniaxial cyclic compression", *Int. J. Geomech.*, **20**(9), 04020159. https://doi.org/10.1061/(ASCE)GM.1943-5622.0001801.

Vásárhelyi, B. and Ván, P. (2006), "Influence of water content on the strength of rock", *Eng. Geol.*, **84**(1-2), 70-74. https://doi.org/10.1016/j.enggeo.2005.11.011.

Vishal, V., Ranjith, P.G. and Singh, T.N. (2015), "An experimental investigation on behaviour of coal under fluid saturation, using acoustic emission", *J. Nat. Gas Sci. Eng.*, **22**, 428-436. https://doi.org/10.1016/j.jngse.2014.12.020.

Wang, B., Jiang, F.X., Zhu, S.T., Zhang, X.F., Shang, X.G., Gu, S.Y. and Wu, Z. (2020a), "Investigating on the mechanism and prevention of rock burst induced by high intensity mining of drainage area in deep mines", *J. China Coal Soc.*, **45**(9), 3054-3064. https://doi.org/10.13225/j.cnki.jccs.2020.0382.

Wang, S., Li, H.M., Wang, W. and Li, D.Y. (2018b), "Experimental study on mechanical behavior and energy dissipation of anthracite coal in natural and forced water-saturation states under triaxial loading", *Arabian J. Geosci.*, **11**(21), 1-17. https://doi.org/10.1007/s12517-018-4014-4.

Wang, W., Zhang, S.W., Wang, S., Li, D.Y., Wang, W., Hao, Y.X. and Wang, H. (2021), "Mechanical behavior of limestone in natural and forced saturation states under uniaxial loading: an experimental study", *Geomech. Geophys. Geo-Energy Geo-Resources*, **7**, 65. https://doi.org/10.1007/s40948-021-00261-6.

Wang, X.R., Wang, E.Y., Liu, X.F., Li, X.L., Wang, H. and Li, D.X. (2018a), "Macro-crack propagation process and corresponding AE behaviors of fractured sandstone under different loading rates", *Chinese J. Rock Mech. Eng.*, **37**(6), 1446-1458. https://doi.org/10.13722/j.cnki.jrme.2017.1672.

Wang, Z. H., Bi, L.P., Kwon, S., Qiao, L.P. and Li, W. (2020b), "The effects of hydro-mechanical coupling in fractured rock mass on groundwater inflow into underground openings", *Tunn. Undergr. Sp. Tech.*, **103**, 103489. https://doi.org/10.1016/j.tust.2020.103489.

Xu, J.Z., Zhai, C., Qin, L. and Liu, S.M. (2018), "Pulse hydraulic fracturing technology and its application in coalbed methane extraction", *Int. J. Oil Gas Coal Tech.*, **19**(1), 115-133. https://doi.org/10.1504/IJOGCT.2018.093962.

Yang, J., Hatcherian, J., Hackley, P.C. and Pomerantz, A.E. (2017), "Nanoscale geochemical and geomechanical characterization of organic matter in shale", *Nature Commun.*, **8**(1), 2179. https://doi.org/10.1038/s41467-017-02254-0.

Yang, X.H., Ren, T., Tan, L.H. and Remennikov, A. (2021), "Effects of water saturation time on energy dissipation and burst propensity of coal specimens", *Geomech. Eng.*, **24**(3), 205-213. https://doi.org/10.12989/gae.2021.24.3.205.

Yao, Q.L., Zheng, C.K., Tang, C.J., Xu, Q., Chong, Z.H. and Li, X.H. (2020), "Experimental investigation of the mechanical failure behavior of coal specimens with water intrusion", *Front. Earth Sci.*, **7**, 348. https://doi.org/10.3389/feart.2019.00348.

Yu, J.L., Tahmasebi, A., Han, Y.N., Yin, F.K. and Li, X.C. (2013), "A review on water in low rank coals: the existence, interaction with coal structure and effects on coal utilization", *Fuel Process. Tech.*, **106**, 9-20. https://doi.org/10.1016/j.fuproc.2012.09.051.

Yuan, R.F., Li, Y.Q. and Jiao, Z.H. (2015), "Movement of overburden stratum and damage evolution of floor stratum during coal mining above aquifers", *Procedia Eng.*, **102**:1857-1866. https://doi.org/10.1016/j.proeng.2015.01.324.

Zhang, T., Yu, L.Y., Su, H.J., Zhang, Q. and Chai, S.B. (2021), "Experimental and numerical investigations on the tensile mechanical behavior of marbles containing dynamic damage", *Int. J. Min. Sci. Tech.*, **32**(1), 89-102. https://doi.org/10.1016/j.ijmst.2021.08.002.

Zhang, Y.T., Ding, X.L., Huang, S.L., Wu, Y.J. and He, J. (2020), "Strength degradation of a natural thin-bedded rock mass subjected to water immersion and its impact on tunnel stability", *Geomech. Eng.*, **21**(1), 63-71. https://doi.org/10.12989/gae.2020.21.1.063.

Zhou, K.Y., Dou, L.M., Gong, S.Y., Li, J.Z., Zhang, J.K. and Cao, J.R. (2020b), "Study of rock burst risk evolution in front of deep longwall panel based on passive seismic velocity tomography", *Geofluids*, **2020**(1), 1-14. https://doi.org/10.1155/2020/8888413.

Zhou, K.Y., Dou, L.M., Li, X.W., Song, S.K., Cao, J.R., Bai, J.Z. and Ma, X.T. (2022), "Coal burst and mining-induced stress evolution in a deep isolated main entry area - A case study", *Eng. Fail. Anal.*, **137**, 106289. https://doi.org/10.1016/j.engfailanal.2022.106289.

Zhou, Z.L., Tan, L.H. and Cai, X. (2020a), "Water infusion on the stability of coal specimen under different static stress conditions", *Appl. Sci.*, **10**(6), 2043. https://doi.org/10.3390/app10062043.